A Reconfigurable Multimode Demultiplexer/Switch for Mode-Multiplexed Silicon Photonics Interconnects

Rubana B. Priti, *Student Member, IEEE*, and Odile Liboiron-Ladouceur, *Senior Member, IEEE*

***Abstract*—We experimentally demonstrate a scalable and broadband reconfigurable multimode demultiplexer/switch (RMDS) for mode-division multiplexed inter- and intra-chip data communication systems. The RMDS exploits a thermo-optically tuned tapered multimode interference coupler, enabling simultaneous transmission of the fundamental and first order quasi transverse electric modes in C-band. It is used as the building block in a mode demultiplexer with −20 dB crosstalk, which can be reconfigured as a mode selecting switch with 10.9 μs switching time. An aggregated bandwidth of 2 × 10 Gb/s is achieved by the parallel transmission of two nonreturn-to-Zero (NRZ) PRBS31 data signals at 10^{-12} bit-error-rate with 2.8 dB BER power penalty. A 1.55 pJ/bit energy efficiency is estimated for a proposed multimode optical link.**

***Index Terms*—Silicon photonics, Photonic integrated circuits, Optical packet switching, Optical interconnections.**

I. Introduction

COMPUTATIONAL speed and complexity of high performance computing systems in data centers are rapidly increasing to keep pace with the skyrocketing demand of global IP traffic. Bandwidth density and energy consumption are two key concerns in modern data centers, where hundreds of thousands of massively parallel computers are interconnected to facilitate high speed parallel data movement [1]. Optical interconnect using complementary metal oxide (CMOS) compatible silicon photonics is evolving as a promising solution to diminish this communication bottleneck, enabled by low-cost and mature silicon-on-insulator (SOI) fabrication and processing technology [2]. In inter- and intra-chip data communications, wavelength-division-multiplexing (WDM) requires multiple lasers and optical filters for each communicating channel imposing cost and complexity. Alternate multiplexing schemes such as polarization-division-multiplexing (PDM), space-division-multiplexing (SDM), and mode-division-multiplexing (MDM), along with WDM, are being developed for greater bandwidth density, higher aggregated channel capacity, and better energy efficiency in chip scale silicon photonics systems [3].

The unique potential of MDM lies on the orthogonality of different eigenmodes inside an SOI waveguide. The large refractive index contrast between propagating (Si) and surrounding (SiO_2) materials allow simultaneous parallel data transmission over a single physical channel. The optical link capacity is increased with a better potential of scalability and energy consumption [4]. However, mitigating inter-modal crosstalk is challenging in the MDM approach due to continuous overlap among different propagating modes, which requires more robust design of on-chip photonic components and devices. In recent years, significant research effort is given towards the development of on-chip MDM links. Mode converters using tapered waveguides [5] and mode-selective filters using directional couplers [6] are reported. Multimode (de)multiplexers are demonstrated using adiabatic directional couplers (ADC) [7], [8], micro ring resonators (MRR) [9], multimode interference (MMI) couplers [10], and both symmetric [11] and asymmetric [12] Y-junctions. WDM and MDM are combined demonstrating 4.35 Tb/s aggregated data transmission over 87 WDM channels using MRR and tapered directional couplers [13]. A 64-channel hybrid (de)multiplexer is reported using arrayed wavelength gratings (AWG) and ADC [14]. WDM compatible multimode switching is demonstrated using MRR [15], [16] and Mach-Zenhder interferometer (MZI) [17]. On-chip MDM link exploiting the propagation of optical supermode using closely-spaced SOI waveguides is reported [18], [19], [20]. Recently, we demonstrated a high-speed mode switch with 2.5 ns switching time using a symmetric Y-junction [21].

We recently also demonstrated an on-chip mode-selecting switch (MSS) [22] comprising of cascaded MMI couplers and thermo-optic phase-shifters. A mode decomposer MMI is the most critical component of the MSS providing the required modal separation and channel crosstalk. In this paper, we demonstrate a novel scalable and broadband reconfigurable mode demultiplexer/switch (RMDS) using this mode decomposer as the building block of a mode demultiplexer and a mode switch. The proof-of-concept device can concurrently transmit and switch high speed optical data over the fundamental and the first order quasi-transverse electric (quasi-TE) modes. The quasi-TE0 and quasi-TE1 modes are launched using only one C-band laser (from 1500 nm to 1600 nm) improving the energy

Manuscript received January 28, 2018; revised May 10, 2018; accepted May 15, 2018. Date of publication May 24, 2018; date of current version June 7, 2018. This work was supported in part by the Natural Sciences and Engineering Research Council (NSERC) SiEPIC CREATE program, in part by the Canada Research Chair program, and in part by the Department of Electrical and Computer Engineering at McGill University. *(Corresponding author: Rubana B. Priti.)*

The authors are with the Department of Electrical and Computer Engineering, McGill University, Montreal, QC H3E 0E9, Canada (e-mail: rubana.priti@mail.mcgill.ca; odile@ieee.org).

Color versions of one or more of the figures in this paper are available online at http://ieeexplore.ieee.org.

Digital Object Identifier 10.1109/JSTQE.2018.2840421

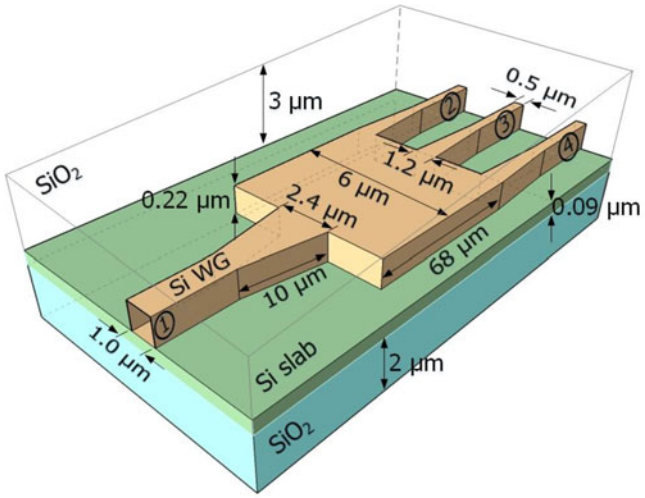

Fig. 1. Schematic of the RMDS in 3D view with input *port 1* and output *port 2, port 3,* and *port 4.*

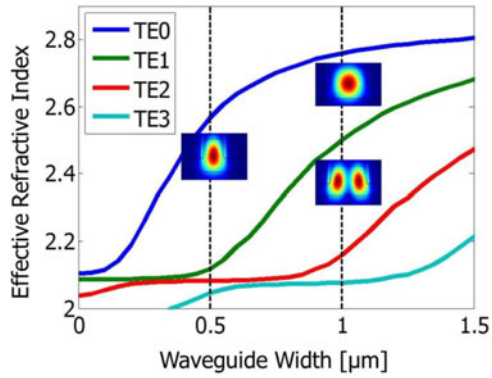

Fig. 2. Simulated effective refractive index as a function of waveguide width inside a 220 nm × 550 nm SOI rib waveguide with a 90 nm slab at 1550 nm.

efficiency. Parallel data transmission is confirmed by the simultaneous transmission of two individual nonreturn-to-zero (NRZ) data packets at 10 Gb/s. For mode demultiplexing, a mode combiner stage is needed after the RMDS to retrieve the input TE0 and TE1 modes. This mode combiner is replaced by a mode switching MMI in the MSS as reported in [22]. As the propagation and manipulation of different eigenmodes in a waveguide is critically related to the dimension of the photonic components, which makes it difficult to manipulate different mode orders in the same structure, the quasi-TE1 mode is decomposed to its fundamental (^{0}TE1) components before processing. Distortion free data transmission is demonstrated for 2×10 Gb/s aggregated bandwidth with a bit-error-rate (BER) of 10^{-12} and $<$2.8 dB power penalty while simultaneously transmitting two data channels.

II. Design and Working Principle of the Reconfigurable Mode Demultiplexer/Switch (RMDS)

The 3D schematic of the proposed RMDS is shown in Fig. 1. The RMDS is a 1×3 MMI coupler consisting of a multimode input port (*port 1*) and three single-mode output ports (*port 2*, *port 3* and *port 4*). For the single-mode transmission, either the fundamental (quasi-TE0) or the first-order (quasi-TE1) mode is launched at *port 1*. The input TE0 mode is mapped onto *port 3* as ^{0}TE0 with a smaller mode-field diameter (MFD). The input TE1 mode is decomposed into two fundamental mode components of equal amplitudes but with opposite phases. These mode components are mapped to *port 2* and *port 4* as ^{0}TE1. For the multimode transmission, both the TE0 and the TE1 modes are launched simultaneously at *port 1* and separated at the output ports into their fundamental mode components. The ^{0}TE0 component from TE0 mode is mapped to *port 3*, and the ^{0}TE1 components from TE1 mode are mapped to *port 2* and *port 4*.

A 220 nm thick SOI waveguide core with a 90 nm thick silicon slab is used for guiding and propagating the optical signal. The waveguides are buried in between a 2 μm thick bottom oxide layer and a 3 μm thick top oxide cladding layer. A commercial simulation tool from Lumerical is used for modeling the effective refractive indices of the first four quasi-TE modes (TE0, TE1, TE2 and TE3) as a function of waveguide widths (Fig. 2). The cutoff widths of the access waveguides for the single-mode (TE0) and the multimode (TE0+TE1) transmissions are 0.5 μm and 0.8 μm, respectively. The effective refractive index is less sensitive to the waveguide width variation for a wider waveguide resulting in greater robustness against process variation. For this reason, the width of the multimode waveguide is optimized to be 1.0 μm.

In the MZI based devices, a small imbalance in the power coupling ratios between the coupler's output ports contributes to large degradation in the crosstalk. Wider waveguide widths make MMI couplers more viable against fabrication process variations compared to adiabatic directional couplers. Hence, MMI couplers exhibit lower coupling power imbalance leading to higher extinction ratio ($>$25 dB) and lower crosstalk [23]. In addition, the lengths of adiabatic couplers increase with the number of modes, which challenges scalability to greater number of modes.

For a fixed MMI width of 6 μm, the estimated beat length (L_π) of 90 μm and input/output locations of the MMI coupler are calculated by using the analytical equations in [24]. Like a mode filter with 100% mode conversion efficiency, the RMDS maps the symmetric (TE0) and the asymmetric (TE1) modes to the different output waveguides. For the symmetric mode, we applied the theory of symmetric interference, where the input that is launched at the center of the MMI forms the *M*-th *N*-fold image at a distance, L_{MMI}, defined by [25]

$$L_{MMI} = \frac{M}{4N}(3L_\pi) \tag{1}$$

The principle of general interference is applied for the asymmetric mode which satisfies the length, L_{MMI}, as long as the single-mode input waveguide is not positioned at the center of the MMI [26]. Considering the wider multimode input waveguide (1.0 μm wide) as two single mode waveguides (0.5 μm wide) placed next to each other, this condition is satisfied. To obtain the first ($M = 1$) single image ($N = 1$), the MMI length (L_{MMI}) becomes $\frac{3}{4}L_\pi$.

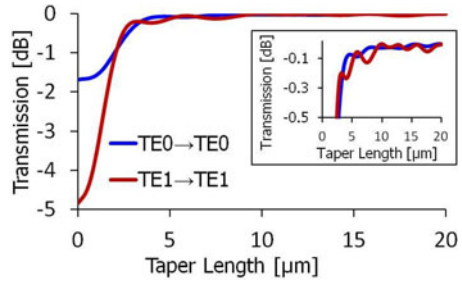

Fig. 3. Simulated optical transmission of TE0 and TE1 modes in the input taper of the RMDS as a function of taper length. The inset is the zoomed-in of the peak optical powers.

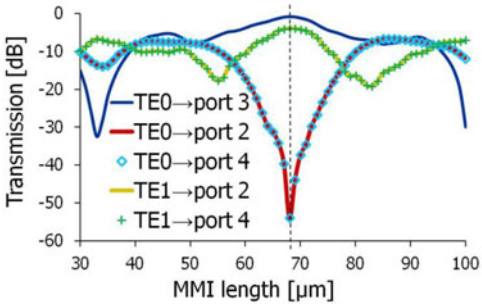

Fig. 4. Simulated optical power of TE0 and TE1 mode components as a function of the length of the RMDS at 1550 nm wavelength. The *TE1→ port 3* transmission exhibits negligible transmittance (<-250.0 dB) IL hence not shown.

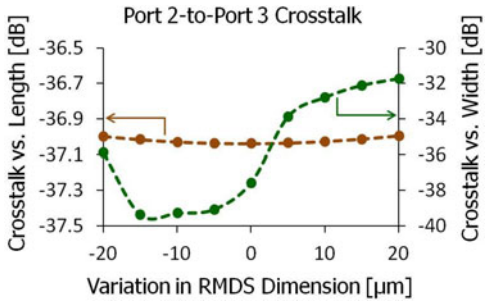

Fig. 5. Simulated crosstalk between *port 2* and *port 3* as a function of the variation of RMDS dimensions (length and width) for TE0 transmission. The initial length and width representing 0 μm variation are 68 μm and 6 μm, respectively.

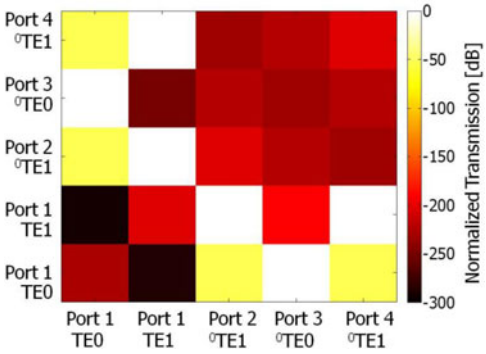

Fig. 6. Simulated optical S-matrix of the 68 μm long RMDS for the transmission of TE0 and TE1 mode components.

Optical reflection and scattering losses at the input and output ends are minimized by adding 10 μm long tapers, which allow more than 98% transmissions of both TE0 and TE1 modes satisfying adiabatic condition [27]. The normalized transmission of the TE0 and the TE1 modes at the input taper (*port 1*) of the RMDS is shown in Fig. 3, confirming adiabatic transmission of both modes. The inset is the zoomed-in of the peak transmission. The length of the RMDS is optimized by the fully vectorial and bi-directional eigenmode expansion model. The simulated transmission as a function of MMI length is shown in Fig. 4 for a 0 dBm Gaussian beam optical input at 1550 nm. There are three scenarios when the input optical signal is launched at *port 1* of the RMDS:

1) Single-mode (TE0) transmission: maximum power in *port 3* with minimum power in both *port 2* and *port 4*.
2) Single-mode (TE1) transmission: maximum power in both *port 2* and *port 4* with minimum power in *port 3*.
3) Multimode (TE0+TE1) transmission: maximum power in all of *port 2*, *port 3,* and *port 4*.

From Fig. 4, these conditions are satisfied for an RMDS length of 68 μm when the *TE0-to-port3* transmission, and both *TE1-to-port2* and *TE1-to-port4* transmissions are maximum, and the *TE0-to-port4* transmission is minimum. It is observed in Fig. 4 that TE0 transmissions at *port 2* and *port 4* are sensitive to MMI length. Although MMI's are more tolerant to fabrication process variation than single mode (0.5 μm wide) waveguides, a small change in the MMI dimension can result in large crosstalk between *port 3* and *port 2* or between *port 3* and *port 4*. As $\pm$10 nm change in dimension can be expected from the fabrication error [28], the crosstalk between *port 3* and *port 2* for TE0 transmisison is estimated within $\pm$20 nm range, and shown in Fig. 5 as a function of RMDS length and width variations. The initial length and width are 68 μm and 6 μm, respectively, representing 0 μm variation. Negligible change in crosstalk is observed with length variation. However, crosstalk increases from -39.4 dB to -31.7 dB with the width variation, although remains <-31 dB within this range.

The simulated scattering matrix (S-matrix) including all possible input/output combinations of all mode components for a 68 μm long RMDS is shown in Fig. 6 when a multimode (TE0+TE1) optical signal of 0 dBm (1 mW) input power is launched at *port 1*. The power leakage at *port 2* and *port 4* from the TE0 input is comparatively higher (-53 dBm) than the leakage at *port 3* from the TE1 input (-190 dBm). Although the simulation accounts for multiple reflection events, it does not take into account the scattering losses from waveguide sidewall roughness and uneven waveguide surfaces leading to these unrealistic values of leakage power. However, these simulation results remain valuable in providing information on relative crosstalk among the output ports. As the beam divergence of a propagating Gaussian beam is inversely proportional to the beam radius at its launching point [29], the higher leakage at *port 2* and *port 4* may result from the higher MFD of the TE0 mode than that of TE1 mode at *port 3*. Very small back reflection ($\sim 10^{-2}$ dB) is expected at each port leading to small

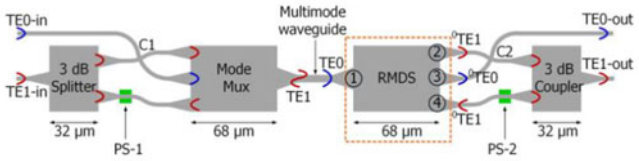

Fig. 7. Schematic of the mode demultiplexer. The electric fields and the optical transmissions of the RMDS delimited by the orange box, is shown in Fig. 8.

optical return loss. Note that higher order quasi-TE (e.g., TE2, TE3, etc.) and quasi-TM (e.g., TM0, TM1, etc.) modes are not considered in the simulation, assuming little inter-modal power leakage from these modes. In reality, these unexpected modes affect the net transmission at each output port. This will be discussed in the next section. As the RMDS is demonstrated as a proof-of-concept device using TE0 and TE1 modes, we will limit our discussion to TE0 and TE1 modes.

III. Mode Demultiplexing

The mode demultiplexer (MD) requires four cascaded MMIs (a 3-dB splitter, a mode multiplexer, the RMDS, and a 3-dB coupler), and two resistive heater phase-shifters (PS-1 and PS-2), as shown in Fig. 7. The phase-shifters are used for tuning the relative phases of the ^{0}TE1 components for multiplexing and demultiplexing the TE1 mode to and from the multimode waveguide, respectively. Note that the transmission of the TE0 mode does not require a phase-shift. Each phase-shifter is 250 μm long consisting of highly N-doped (N++) silicon slab placed 700 nm away from the waveguide core. The detailed design of the phase-shifter can be found in [30].

A. Design and Working Principle

As a mode mux and a mode demux are identical devices with opposite input/output direction, a single bi-directional component can be designed for both multiplexing and demultiplexing operations. The simulated electrical fields in the RMDS are shown in Fig. 8(a), (c) and (e) for the single channel transmission of TE0 mode, single channel transmission of TE1 mode, and dual channel transmission (TE0+TE1) mode, respectively. The net optical transmissions from 1500 nm to 1600 nm corresponding to each mode are shown in Fig. 8(b), (d) and (f), respectively.

For the single channel transmission, either the *TE0 in* or the *TE1 in* input ports (Fig. 7) are used for the transmission of the TE0 mode or the TE1 mode, respectively. For the TE0 transmission, the input light is coupled to the middle input port of the mode mux and mapped to its multimode output port with a larger MFD. The RMDS maps this beam to its *port 3* output port as ^{0}TE0, shown in Fig. 8(a), without any decomposition to retrieve the original optical signal at the *TE0 out* output port. A -29 dB crosstalk is estimated at 1550 nm with -1.5 dB insertion loss (IL), as shown in Fig. 8(b). This crosstalk is higher than that of Figs. 4 and 6, where only TE0 and TE1 modes are considered for the length optimization. However, in reality, higher order quasi-TE and quasi-TM modes may cause power leakage and inter-mode cross-coupling resulting in crosstalk degradation.

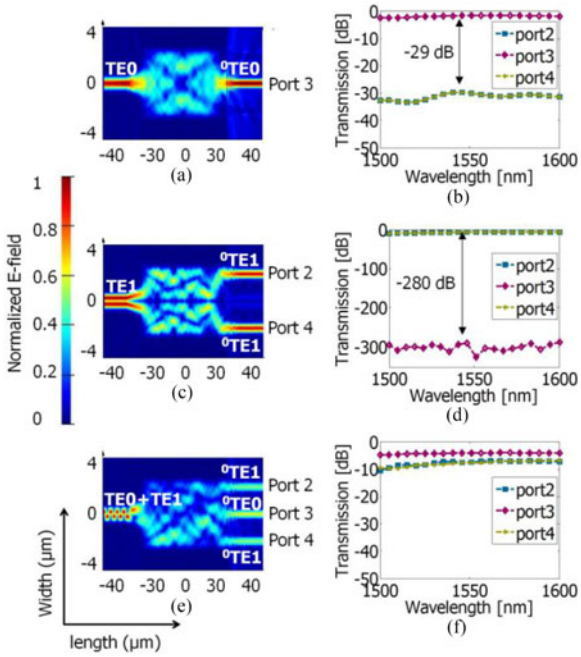

Fig. 8. Simulated electric fields (left) and optical transmissions (right) of the RMDS, marked by the orange box in Fig. 6. The top (a, b), middle (c, d) and bottom (e, f) images represent the single channel TE0, single channel TE1, and dual channel (TE0+TE1) transmissions.

For the TE1 transmission, the 3-dB splitter separates the optical input into two fundamental mode components with the same phase as the original input signal, corresponding to a phase-shift of $\Delta\varphi = 0$. As the two mode components of a TE1 mode are out-of-phase by π rad, a phase-shift of $\Delta\varphi = \pi$ is applied to one of the mode components by thermo-optically tuning the PS-1 phase-shifter. These two π-phase-shifted components are coupled to the upper and the lower input ports of the mode mux and mapped as TE1 mode to its multimode output port. The RMDS then decomposes the two mode components as ^{0}TE1 at its *port 2* and *port 4* output ports, as shown in Fig. 8(c). These two mode components are phase-matched by the PS-2 phase-shifter, recombined by the 3-dB coupler, and retrieved at the *TE1 out* output port with simulation results estimating insignificant crosstalk (<-280 dB) and an IL ranging from -6.3 dB to -9.0 dB in C-band (1500 nm–1600 nm), as shown in Fig. 8(d).

For dual channel transmission, the CW input from a single laser is power divided by an off-chip 50/50 power splitter to simultaneously couple two optical signals to both the *TE0 in* and the *TE1 in* input ports. The RMDS decomposes the multimode (TE0+TE1) signal and maps the ^{0}TE0 component to *port 3*, and the two ^{0}TE1 components to *port 2* and *port 4*, respectively (Fig. 8(e)). The simulated IL obtained are -7.3 dB, -4.0 dB and -7.5 dB at *port 2*, *port 3* and *port 4*, respectively, as shown in Fig. 8(f). The degradation in IL may arise from the inter-mode cross-coupling between the TE0 and the TE1 modes while propagating through the multimode waveguide. This may cause a power leakage in the net transmission of the corresponding modes at the output ports.

The MD was fabricated using 193 nm deep ultraviolet (DUV) lithography at the Institute of Microelectronics (A*STAR IME),

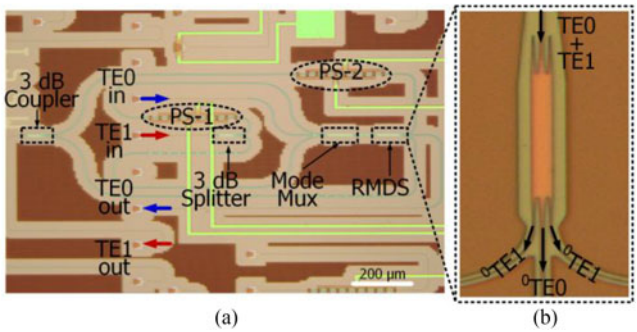

Fig. 9. (a) Optical micrograph of the fabricated chip of the mode demultiplexer using the RMDS; (b) zoomed-in optical micrograph of the RMDS.

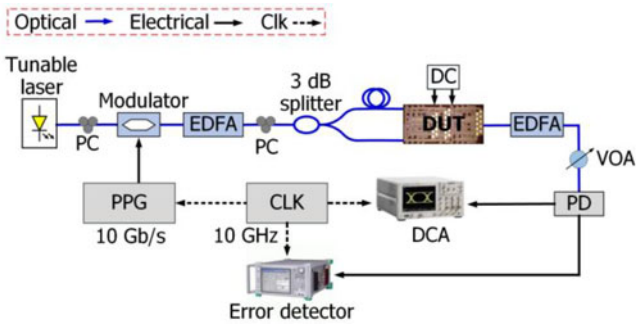

Fig. 10. Experimental setup for the mode demultiplexer measurement. The optical and the electrical connections are shown as blue and black lines, respectively. EDFA: Erbium doped fiber amplifier, PC: polarization controller, DUT: device under test, VOA: Variable optical attenuator, PD: photodetector, DCA: digital communication analyzer, PPG: Programmable pattern generator, CLK: clock synthesizer. The DCA and error detector are not connected at the same time to the photodetector.

through a multi-project wafer (MPW) service managed by Canadian Microelectronic Corporation (CMC) Microsystems. The optical microscope image of the fabricated chip is shown in Fig. 9(a). Although two waveguide crossings at C1 and C2 are shown in the schematic in Fig. 7, these crossings are removed in the design layout by unfolding the input and output waveguides, and routing them around the grating coupler array to reduce inter-mode cross-coupling. Indeed, this modification in the device layout increases the total device footprint which can be reduced by using a low-loss waveguide crossing. Fig. 9(b) is a zoomed-in view of the fabricated RMDS, which is designed as a 3×3 MMI coupler using the principle of general interference but fabricated as a 1×3 MMI, where 30 μm long tapers are added at the unused ports to reduce the reflection loss.

B. Experimental Results

The experimental setup to validate the fabricated chip is shown in Fig. 10. First, the MD is characterized with a CW optical signal using a tunable laser source (Yenista Tunics T100R). On-chip surface grating couplers with a 3-dB bandwidth of 47 nm at 1550 nm vertically couple the continuous wave (CW) optical signal at the fundamental mode from the laser through a fiber-array. For the single channel measurement, the input power is 0 dBm. For the dual channel measurement, the input

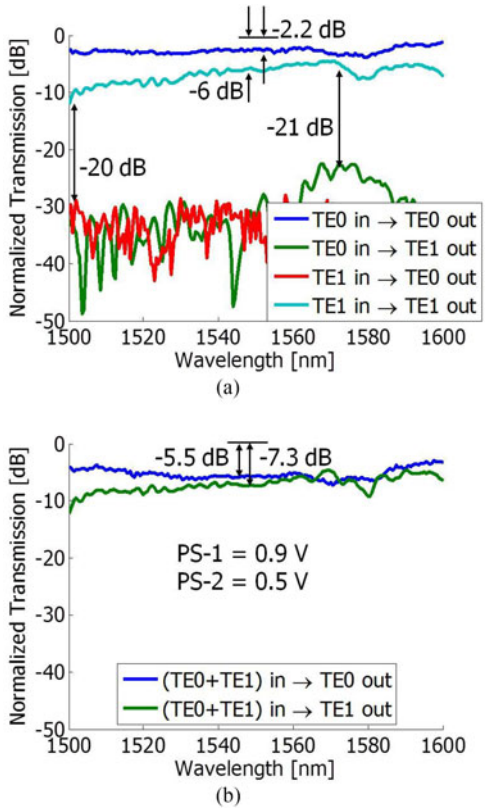

Fig. 11. Normalized optical transmission of the (a) single channel and (b) dual channel transmission of the mode demultiplexer as a function of wavelength.

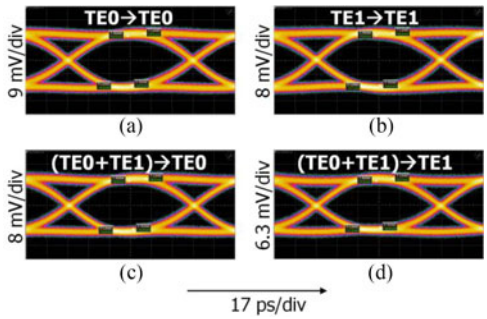

Fig. 12. Recorded eye diagram of the mode demultiplexer for the single channel (top) and dual channel (bottom) inputs.

power is increased to 3 dBm to compensate for the 50/50 splitter. The decorrelation of two channels was performed through an SMF-28 fiber delay line providing 480 bit delay between two propagating channels (>16-bit minimum walk-off requirement [31]). A short waveguide connecting two vertical grating couplers is used as a reference structure for the fiber-to-fiber insertion loss (IL) measured to be -10.5 dB at 1550 nm. The optical transmissions are normalized to the IL of this reference waveguide.

The optical transmissions as a function of wavelength for both single channel and dual channel are shown in Fig. 11. For the single channel transmission at 1550 nm (Fig. 11(a)), the IL for the TE0 mode (*TE0 in* $\rightarrow$ *TE0 out*) is -2.2 dB, and for the TE1 mode (*TE1 in* $\rightarrow$ *TE1 out*) it is -6.0 dB. As the TE1 mode

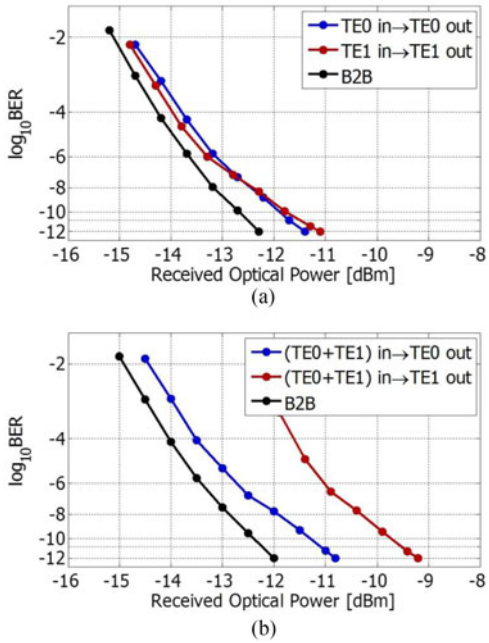

Fig. 13. Measured BER (log-scale) of the demultiplexer for (a) single channel and (b) dual channel transmissions as a function of average optical power (dBm), received by a 20 GHz photoreceiver of −18 dB sensitivity and 0.8 A/W responsivity.

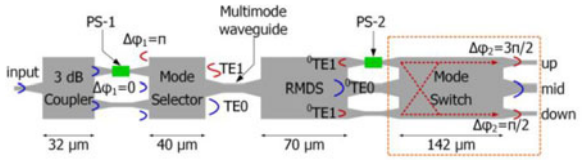

Fig. 14. Schematic of the MSS using the RMDS as the mode decomposer. The mode switch MMI, simulated in Fig. 15, is marked by an orange line.

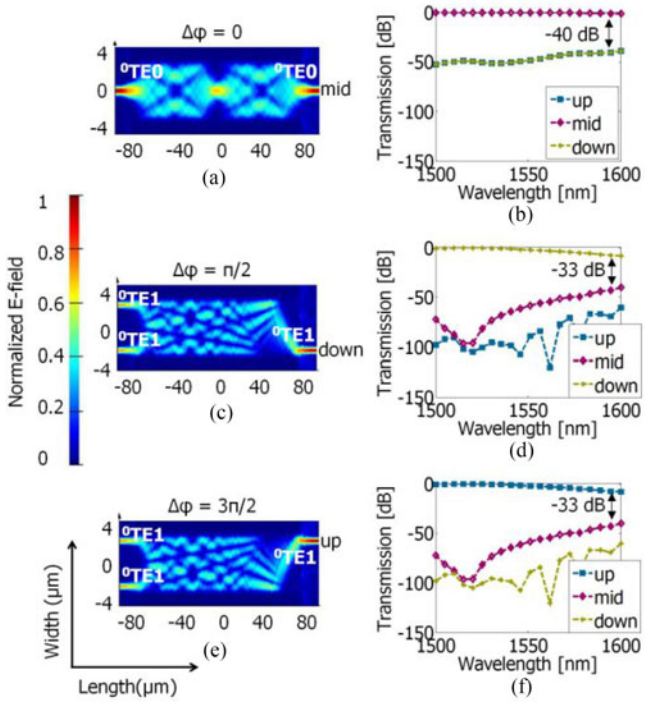

Fig. 15. Simulated electric fields (left) and optical transmissions (right) of the mode switch MMI, marked by an orange line in Fig. 14. The *mid* (a, b) channel corresponds to TE0 ($\Delta\varphi = 0$) transmission. The *down* (c, d) and *up* (e, f) channels correspond to TE1 transmissions for $\Delta\varphi = \pi/2$ and $\Delta\varphi = 3\pi/2$ phase-shifts.

propagates with a lower effective refractive index than the TE0 mode (Fig. 2), it is likely that the corresponding TE1 optical beam is less confined inside the multimode waveguide with a longer evanescent tail being outside the waveguide core. This may lead to higher IL for the TE1 mode. The crosstalks for the TE0 transmission (*TE0 in → TE1 out*) is less than −21.0 dB and that for TE1 transmission (*TE1 in → TE0 out*) is less than −20.0 dB over 100 nm wavelength range. For the dual channel transmission (Fig. 11(b)), the TE0 and TE1 modes exhibit −5.5 dB and −7.3 dB IL, respectively. The higher IL in the multimode transmission indicates inter-mode cross-coupling between TE0 and TE1 modes, and possibly modal leakage of the higher order quasi-TE (e.g., TE2, TE3) and quasi-TM (e.g., TM0, TM1) modes. Although the effective refractive indices of these modes are very small (<1.95 for the strip waveguide as reported in ref. [3]) resulting in negligible optical power transmission, these undesired modes may cause the leakage of optical power from the dominant TE0 and TE1 modes leading to higher loss.

For payload data transmission, a 10 Gb/s NRZ PRBS-31 signal is generated by an Anritsu MP 1800A pulse pattern generator (PPG). A modulated and amplified optical input signal is coupled to the device under test (DUT) in quasi-TE polarization, maintained by a polarization controller (PC). The output is detected by a 20 GHz photodetector (PD) of −18 dB sensitivity. For the back-to-back (B2B) BER measurement, reported in Fig. 13(a) and (b), the DUT is replaced by an optical attenuator (VOA) with the corresponding loss of the *TE0 out* transmission in both cases. An Anritsu 20 GHz signal generator is used as the clock synthesizer to provide the external clock to the PPG and the error detector, and the trigger to the Agilent 86100C digital communication analyzer (DCA) for recording eye diagrams. The eye diagrams in Fig. 12(a) and (b) are recorded for single channel inputs in the TE0 (*TE0 in → TE0 out*) and the TE1 (*TE1 in → TE1 out*) transmissions, respectively. For the dual channel input (TE0+TE1), the optical payload is transmitted simultaneously over both TE0 and TE1 modes and the eye diagrams are recorded at the *TE0 out* and *TE1 out* output ports, shown in Fig. 12(c) and (d), respectively. Clear and open eyes are observed in all channels demonstrating distortion-free high-speed data transmission for both TE0 and TE1 modes.

The measured BER as a function of the average received optical power is shown in Fig. 13(a) for the single channel and in Fig. 13(b) for the dual channel transmissions along with the back-to-back (B2B) conditions in both cases. A BER of 10^{-12} is observed for all channels at an aggregated data rate of 2×10 Gb/s demonstrating error free data transmission. The power penalties in the single mode transmission (Fig. 11(a)) are 0.9 dB and 1.1 dB in the *TE0 out* and the *TE1 out* output ports, respectively. The cascaded MMI structures are likely causing

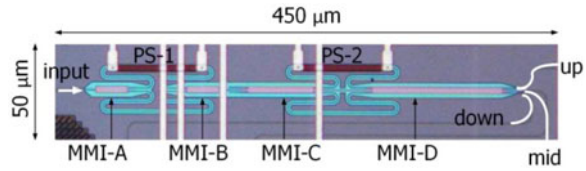

Fig. 16. Optical micrograph of the fabricated MSS of 450 μm × 50 μm footprint area.

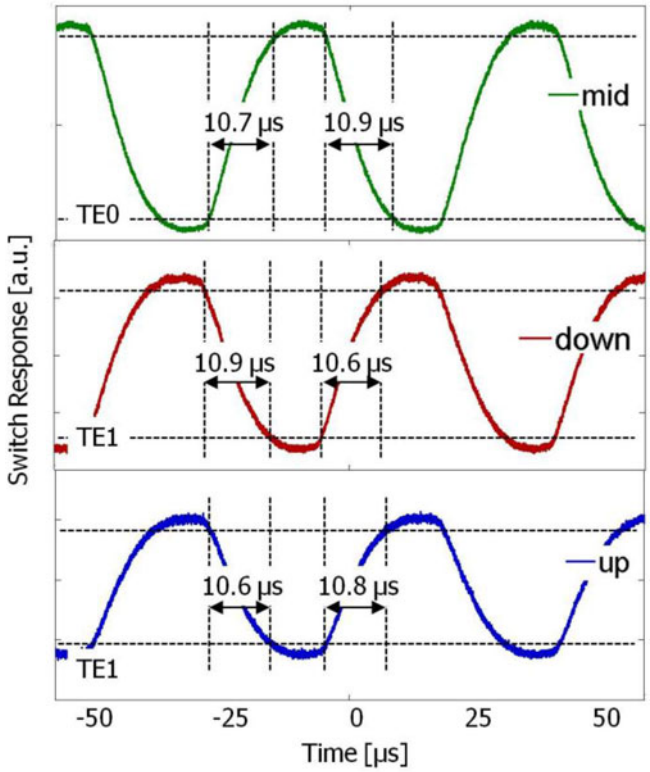

Fig. 17. Measured on-off-keying (OOK) switching response of the MSS for the switching of the TE0 (*mid*) and the TE1 (*down* and *up*) modes.

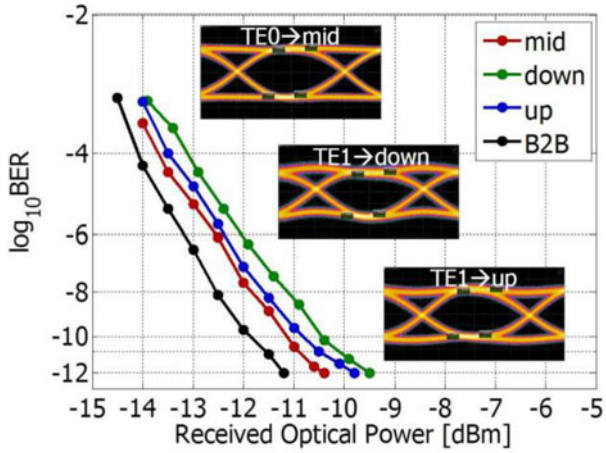

Fig. 18. Measured BER at *mid*, *down* and *up* output ports of the MSS as a function of the average received optical power by the same photoreceiver as in Fig. 13.

greater inter-modal cross-coupling to higher-order modes (TE2 and higher) resulting in BER power penalties. In dual channel transmission, the power penalties are 1.2 dB for the TE0 mode and 2.8 dB for the TE1 mode. The increase in BER power penalties is assumed to be the effect of higher order inter-mode cross-coupling and associated increase in IL in the multimode transmission as reported in Fig. 11(b). Note that no optical filter is used in the experiment as the filter adds −2 dB insertion loss without significant improvement of electrical SNR and eye-quality. This situation results in higher ASE noise in the photoreceiver which may impact the power penalty.

IV. Mode Switching

The detail design and experimental validation of mode switching operation is reported in [22], where a mode selecting switch (MSS) is realized using the RMDS as a mode decomposer to switch different data channels over TE0 and TE1 modes. Its on-off-keying (OOK) switching characterization and system level performances are used to compare with the MD and to confirm the reconfigurability of the RMDS. The MSS also consists of four cascaded MMIs as in the mode demultiplexer. However, the 3-dB splitter in the MD (Fig. 7) is followed by a mode selector instead of the mode mux, and a mode switching MMI block follows the RMDS replacing the mode coupler. Two over-clad heaters are used as phase-shifters. Each thermally controlled phase shifter consists of 120 nm thick, 100 μm long, and 6 μm wide TiN thin film, designed on [32].

A. Design and Working Principle

A schematic of the mode switch is shown in Fig. 14. Among the two phase-shifters, PS-1 is tuned for selecting either the TE0 or the TE1 mode. The second phase-shifter (PS-2) is tuned for spatially switching the modes among the three output ports of the mode switch MMI. Although the RMDS was designed for 70 μm length in the MSS, we later optimized the length to be 68 μm for better modal separation and less crosstalk. Indeed, this small difference in length was compensated by tuning the PS-2 phase-shifter.

The simulated electric fields of the mode switch MMI for three different phase-shift conditions of the PS-2 are shown in Fig. 15(a), (c) and (e), and the corresponding simulated transmissions are shown in Fig. 15(b), (d) and (f), respectively. For the TE0 transmission, the RMDS maps the mode field as is, to its *port 3* output port as ^{0}TE0 without any decomposition, but with a larger MFD. The mode switch maps it as TE0 to the *mid* output port with no phase-shift ($\Delta\varphi = 0$), as shown in Fig. 15(a). In Fig. 15(b), less than −40 dB crosstalk is estimated with −0.2 dB IL at 1550 nm. For the TE1 transmission, the RMDS decomposes the mode fields as ^{0}TE1 in *port 2* and *port 4*, which are π-out-of-phase with each other. The mode switch recombines the ^{0}TE1 components and switches it to the *down* output ports for $\Delta\varphi = \pi/2$ (Fig. 15(c)) and to the *up* output port for $\Delta\varphi = 3\pi/2$ (Fig. 15(e)). The estimated crosstalk is less than −33 dB and the IL at 1550 nm is −2.0 dB for both *down* and *up* output ports, as shown in Fig. 15(d) and (f), respectively.

TABLE I
EXPERIMENTAL RESULTS OF THE MODE DEMULTIPLEXER (MD) AND THE MODE SELECTING SWITCH (MSS) USING RMDS AS THE BUILDING BLOCK

Parameter	MD				MSS		
Transmission	Single channel		Dual channel		TE0	TE1	
Channel	TE0	TE1	TE0	TE1	mid	down	up
IL (dB)	-6.0	-2.0	-5.5	-7.3	-1.9	-13.5	-13.2
Crosstalk (dB)	-21	-20	_	_	-24	-17	-15
Operating range (nm)	100	100	100	100	95	34	45
Switching time (μs)	_	_	_	_	10.9	10.9	10.8
Electrical power (mW)	0.13	14.7	12.3	12.3	13.6	64.5	123.0
BER Power penalty (dB)	0.9	1.1	1.2	2.8	0.8	1.7	1.4

TABLE II
ESTIMATED POWER BUDGET FOR THE PROPOSED ON-CHIP RMDS BASED MULTIMODE LINK IN DUAL CHANNEL TRANSMISSION AT 2×10 GB/S

Link Component	Electrical Power (mW)	Optical Loss (dB)
Laser	12.0	_
Modulator [29]	3.8	-7.0
Fiber-to-GC coupling	_	-11.0
RMDS (dual channel)	12.3	-7.3
Receiver [29]	3.0	_
Total	31.1	-25.3
Energy efficiency	1.55 pJ/bit	

The MSS was fabricated using the same service as for the MD. An optical microscopic image of the fabricated chip is shown in Fig. 16 with a footprint area of 450 μm $\times$ 50 μm. The footprint area is reduced by folding the waveguides with 7 μm bends forming Mach-Zehnder interferometer (MZI) of 243 μm long arms.

B. Experimental Results

The instrumentation and the testing procedure for the MSS is the same as for the MD except for the switching operation. In the MD, the TE0 and the TE1 modes always appear at the *TE0 out* and *TE1 out* output ports, respectively. However, in the MSS, the TE1 mode is spatially switched between the *down* and the *up* output ports, and the TE0 mode is mapped to the *mid* output port. The *mid*, *down,* and *up* output ports exhibit -1.9 dB, -13.5 dB, and -13.2 dB IL, respectively [22]. For the characterization of dynamic switching performance, a 25.8 kHz electrical square wave is generated by the10 Gb/s Anritsu PPG, and applied as the gating signal for the PS-1 with a 2.1 V peak-to-peak voltage. The switch responses are recorded in real-time using a Keysight InfiniiVision DSO-X-3034A Oscilloscope of 350 MHz bandwidth measuring a 15 ns rise and fall time of the square wave.

Fig. 17 shows the switching of PS-1 between *mid*, *down,* and *up* output ports in response to the gating signal when PS $-$ 2 $=$ 4.2 V. The TE0 signal appears only at the *mid* output port with a measured rise and fall times of 10.7 μs and 10.9 μs, respectively. The TE1 signal switches between the *down* and the *up* output ports. The fall and rise times are 10.9 μs and 10.6 μs, respectively at the *down* output port. For the *up* output port, the fall and rise times are 10.6 μs and 10.8 μs, respectively. The measured BER as a function of received optical power is shown in Fig. 18. A BER of 10^{-12} at an aggregated data rate of 2×10 Gb/s is achieved in all output ports and in the B2B condition. The power penalties for the *mid*, *down* and *up* output ports with respect to the B2B are 0.8, 1.4, and 1.7 dB, respectively. The insets of Fig. 18 show the recorded eye diagrams at all three output ports. Clear and open eyes are observed in all channels demonstrating distortion free high-speed data transmission for both TE0 and TE1 modes.

V. DISCUSSION

The experimental results are summarized in Table I for both the MD and the MSS. The higher IL of -13.5 dB for the TE1 mode in the MSS is due to the destructive interference, applied by the PS-1 phase-shifter, between two input arms of the mode selector MMI (Fig. 14). This is required to cancel the TE0 mode and select TE1 mode for switching. The 10.9 μs switching time can be further improved to 1.8 μs by using resistive heater phase-shifter [33]. The electrical power consumption of the MSS is higher due to the lower thermo-optic tuning efficiency of the TiN heater as measured to be 35.5 mW/π compared to that of resistive heater of 21 mW/π [30]. Although the TE1 output of the dual channel transmission in the MD exhibits higher BER power penalty of 2.8 dB, it is sufficient for a good eye opening as shown in Fig. 10(d), and comparable to the reported value in [17].

To estimate the overall on-chip power consumption of a MDM link, we consider the dual channel transmission of the MD. The on-chip optical power of the laser was measured to be 10.8 dBm (12 mW), excluding the wall-plug efficiency as done in [29]. Considering a reported 3 mW receiver power including a hybrid integrated Ge-on-Si photodetector of -17 dB sensitivity, 0.8 mW electrical power and 3 mW thermal tuning power of a MRR based silicon modulator of -7 dB IL [34] and a measured 12.3 mW thermal-tuning power of the MD, the total power consumption of the link is 31.1 mW at 2×10 Gb/s aggregated data rate. This corresponds to an on-chip energy efficiency of

1.55 pJ/bit, which is less than the reported estimated efficiency of 1.9 pJ/bit [35]. The optical link budget is shown in Table II for this link.

The RMDS can be scaled up to accommodate higher order quasi-TE (e.g., TE2, TE3, etc.) modes by carefully designing its width and length for mapping higher order modes. As each mode component will require some amount of phase-shift for switching and maintaining sufficient crosstalk between demultiplexed signals, the number of phase shifters will increase the total footprint. To compensate a probable increase in the BER power penalty caused by the higher inter-modal cross-coupling of the higher order modes, efficient and low-power phase-shifters are required. Indeed, an experimental verification is needed to determine the plausible mode numbers for a scalable RMDS.

VI. Conclusion

To summarize, we demonstrate a reconfigurable multimode demultiplexer/switch (RMDS) for MDM silicon photonic systems. To the best of our knowledge, this is the first demonstration of such a device that can be reconfigured to perform both mode demultiplexing and mode switching of high speed optical data. An aggregated bandwidth of 2×10 Gb/s is achieved at 10^{-12} BER with less than 2.8 dB power penalty. The RMDS can be scaled up for higher order mode transmission by engineering the length and the width of the MMI with more output ports and phase-shifter stages. A multimode optical link using the RMDS is proposed with an estimated 1.55 pJ/bit energy efficiency. The RMDS can be used as a building block for the deployment of high capacity optical links in short-reach interconnects allowing the parallel transmission and switching of multiple independent data packets for a potential increase in link energy/bit performance.

References

[1] D. A. B. Miller, "Attojoule optoelectronics for low-energy information processing and communications," *J. Lightw. Technol.*, vol. 35, no. 3, pp. 346–396, Feb. 2017.

[2] W. Dargie *et al.*, "A highly adaptive and energy-efficient optical interconnect for on-board server communications," in *Proc. 26th Int. Conf. Comput. Commun. Netw.*, Vancouver, BC, Canada, 2017, pp. 1–8.

[3] D. Dai, J. Wang, and Y. Shi, "Silicon mode (de)multiplexer enabling high capacity photonic networks-on-chip with a single-wavelength-carrier light," *Opt. Lett.*, vol. 38, no. 9, pp. 1422–1424, 2013.

[4] D. Dai, "Silicon nanophotonic integrated devices for on-chip multiplexing and switching," *J. Lightw. Technol.*, vol. 35, no. 4, pp. 572–587, Feb. 2017.

[5] D. Dai, Y. Tang, and J. E. Bowers, "Mode conversion in tapered submicron silicon ridge optical waveguides," *Opt. Express*, vol. 20, no. 12, pp. 13425–13439, 2012.

[6] S. Bagheri and W. M. J. Green, "Silicon-on-insulator mode-selective add-drop unit for on-chip mode-division multiplexing," in *Proc. 6th IEEE Int. Conf. Group IV Photon.*, San Francisco, CA, USA, 2009, pp. 166–168.

[7] X. Wu, C. Huang, K. Xu, C. Shu and H. K. Tsang, "Mode-division multiplexing for silicon photonic network-on-chip," *J. Lightw. Technol.*, vol. 35, no. 15, pp. 3223–3228, Aug. 2017.

[8] C. Sun, Y. Yu, M. Ye, G. Chen and X. Zhang, "An ultra-low crosstalk and broadband two-mode (de)multiplexer based on adiabatic couplers," *Nature Commun.*, vol. 6, 2016, Art no. 38494.

[9] M. Ye, Y. Yu, G. Chen, Y. Luo, and X. Zhang, "On-chip WDM mode-division multiplexing interconnection with optional demodulation function," *Opt. Express*, vol. 23, no. 25, pp. 32130–32138, 2015.

[10] F. Guo *et al.*, "An MMI-based mode (DE)MUX by varying the waveguide thickness of the phase shifter," *IEEE Photon. Technol. Lett.*, vol. 28, no. 21, pp. 2443–2446, Nov. 2016.

[11] Z. Zhang, Y. Yu, and S. Fu, "Broadband on-chip mode-division multiplexer based on adiabatic couplers and symmetric Y-junction," *IEEE Photon. J.*, vol. 9, no. 2, pp. 1–6, Apr. 2017.

[12] W. Chen *et al.*, "Silicon three-mode (de)multiplexer based on cascaded asymmetric Y junctions," *Opt. Lett.*, vol. 41, no. 12, pp. 2851–2854, 2016.

[13] L.-W. Luo *et al.*, "WDM-compatible mode-division multiplexing on a silicon chip," *Nature Commun.*, vol. 5, 2014, Art no. 3069.

[14] J. Wang, S. Chen, and D. Dai, "Silicon hybrid demultiplexer with 64 channels for wavelength/mode-division multiplexed on-chip optical interconnects," *Opt. Lett.*, vol. 39, no. 24, pp. 6993–6996, 2014.

[15] B. Stern *et al.*, "On-chip mode-division multiplexing switch," *Optica*, vol. 2, no. 6, pp. 530–535, 2015.

[16] M. Ye, Y. Yu, C. Sun, and X. Zhang, "On-chip data exchange for mode division multiplexed signals," *Opt. Express*, vol. 24, no. 1, pp. 528–535, 2016.

[17] H. Jia, T. Zhou, L. Zhang, J. Ding, X. Fu, and L. Yang, "Optical switch compatible with wavelength division multiplexing and mode division multiplexing for photonic networks-on-chip," *Opt. Express*, vol. 25, no. 17, pp. 20698–20707. 2017.

[18] C. Sun, Y. Yu, G. Chen, and X. Zhang, "Silicon mode multiplexer processing dual-path mode-division multiplexing signals," *Opt. Lett.*, vol. 41, no. 23, pp. 5511–5514, 2016.

[19] I. Cerutti, N. Andriolli, and P. Velha, "Engineering of closely packed silicon-on-isolator waveguide arrays for mode division multiplexing applications," *J. Opt. Soc. Amer. B*, vol. 34, pp. 497–506, 2017.

[20] C. Li and D. Dai, "Low-loss and low-crosstalk multi-channel mode (de)multiplexer with ultrathin silicon waveguides," *Opt. Lett.*, vol. 42, no. 12, pp. 2370–2373, 2017.

[21] Y. Xiong, R. B. Priti, and O. Liboiron-Ladouceur, "High-speed two-mode switch for mode-division multiplexing optical networks," *Optica*, vol. 4, no. 9, pp. 1098–1102, 2017.

[22] R. B. Priti, H. P. Bazargani, Y. Xiong, and O. Liboiron-Ladouceur, "Mode selecting switch using multimode interference for on-chip optical interconnects," *Opt. Lett.*, vol. 42, no. 20, pp. 4131–4134, 2017.

[23] K. Solehmainen, M. Kapulainen, M. Harjanne, and T. Aalto, "Adiabatic and multimode interference couplers on silicon-on-insulator," *IEEE Photon. Technol. Lett.*, vol. 18, no. 21, pp. 2287–2289, Nov. 2006.

[24] L. B. Soldano and E. C. M. Pennings, "Optical multi-mode interference devices based on self-imaging: principles and applications," *J. Lightw. Technol.*, vol. 13, no. 4, pp. 615–627, Apr. 1995.

[25] T. Uematsu, Y. Ishizaka, Y. Kawaguchi, K. Saitoh, and M. Koshiba, "Design of a compact two-mode multi/demultiplexer consisting of multimode interference waveguides and a wavelength-insensitive phase shifter for mode-division multiplexing transmission," *J. Lightw. Technol.*, vol. 30, no. 15, pp. 2421–2426, Aug. 2012.

[26] J. Leuthold, R. Hess, J. Eckner, P. A. Besse, and H. Melchior, "Spatial mode filters realized with multimode interference couplers," *Opt. Lett.*, vol. 21, no. 11, pp. 836–838, 1996.

[27] Y. Fu, T. Ye, W. Tang, and T. Chu, "Efficient adiabatic silicon-on-insulator waveguide taper," *Photon. Res.*, vol. 2, no. 3, pp. A41–A44, 2014.

[28] M. Nikdast, G. Nicolescu, J. Trajkovic, and O. Liboiron-Ladouceur, "Chip-scale silicon photonic interconnects: A formal study on fabrication non-uniformity," *J. Lightw. Technol.*, vol. 34, no. 16, pp. 3682–3695, Aug. 2016.

[29] O. Svelto, "*Ray and wave propagation through optical media*," *Principles of Lasers*, 5th ed., New York, NY, USA: Springer-Verlag, 2010, ch. 4, pp. 131–162.

[30] R. B. Priti, Y. Xiong, and O. Liboiron-Ladouceur, "Efficiency improvement of an O-band SOI-MZI thermo-optic matrix switch," in *Proc. IEEE Photon. Conf.*, Waikoloa, HI, USA, 2016, pp. 823–824.

[31] D. F. Grosz and R. J. Essiambre, "On the role of optical fibers as channel decorrelators in system experiments," in *Proc. 13th Annu. Meeting IEEE Lasers Electro-Opt. Soc.*, Rio Grande, PR, USA, 2000, vol. 1, pp. 340–341.

[32] J. F. Creemer *et al.*, "Microhotplates with TiN heaters," *Sens. Actuators A, Phys.*, vol. 148, pp. 416–421, 2008.

[33] R. B. Priti and O. Liboiron-Ladouceur, "A broadband rearrangable non-blocking MZI-based thermo-optic O-band switch in silicon-on-insulator," in *Proc. Adv. Photon. (IPR, NOMA, Sensors, Netw., SPPCom, PS)*, 2017, Paper PM4D.2.

[34] X. Zheng *et al.*, "2-pJ/bit (on-chip) 10-Gb/s digital CMOS silicon photonic link," *IEEE Photon. Technol. Lett.*, vol. 24, no. 14, pp. 1260–1262, Jul. 2012.

[35] A. V. Krishnamoorthy, H. Schwetman, X. Zheng, and R. Ho, "Energy-efficient photonics in future high-connectivity computing systems," *J. Lightw. Technol.*, vol. 33, no. 4, pp. 889–900, Feb. 2015.

Rubana B. Priti (S'13) received the B.Sc. and M.S. degrees in applied physics, electronics and communication engineering from the University of Dhaka, Dhaka, Bangladesh, in 2007 and 2008, respectively, and a second M.S. degree in electrical engineering from South Dakota State University, Brookings, SD, USA in 2013. She is currently working toward the Ph.D. degree in electrical engineering from McGill University, Montreal, QC, Canada, specializing on energy efficient silicon photonics interconnects. Her research interest includes optical interconnects, silicon integrated photonics, and photonic-electronic co-packaging. During the summer of 2017, she worked with Teraxion Inc., Quebec City, QC, Canada, as a Research and Development Intern. She is the recipient of the McGill Engineering Doctoral Award, NSERC SiEPIC doctoral scholarship, and IEEE Photonics Society WIP Travel Grant.

Odile Liboiron-Ladouceur (M'95–SM'14) received the B.Eng. degree in electrical engineering from McGill University, Montreal, QC, Canada, in 1999, and the M.S. and Ph.D. degrees in electrical engineering from Columbia University, New York, NY, USA, in 2003 and 2007, respectively. She is currently an Associate Professor and Canada Research Chair in Photonics Interconnect with the Department of Electrical and Computer Engineering, McGill University. She holds 6 patents (4 issued, 2 pending), and she has coauthored more than 45 peer-reviewed journal papers and more than 95 papers in conference proceedings. Her research interests include optical systems, photonic integrated circuits, and photonic interconnects. She is the 2018 recipient of McGill Principal's Prize for Outstanding Emerging Researcher.